Engineering RHO nanozeolite: controlling the particle morphology, Al and cation content, stability, and flexibility

Edwin B. Clatworthy, Arnold A. Paecklar, Eddy Dib, Maxime Debost, Nicolas Barrier, Philippe Boullay, Jean-Pierre Gilson, Nikolai Nesterenko, Svetlana Mintova

Engineering RHO nanozeolite: controlling the particle morphology, Al and cation content, stability and flexibility

Edwin B. Clatworthy, † Arnold A. Paecklar, †‡ Eddy Dib, † Maxime Debost, †‡ Nicolas Barrier, ‡ Philippe Boullay ‡, Jean-Pierre Gilson †, Nikolai Nesterenko ‖, and Svetlana Mintova †*

† Normandie Université, ENSICAEN, UNICAEN, CNRS, Laboratoire Catalyse et Spectrochimie (LCS), 14050 Caen, France

‡ Normandie Université, ENSICAEN, UNICAEN, CNRS, Laboratoire de Cristallographie et Science des Matériaux (CRISMAT), 14050 Caen, France

‖ Total Research and Technologies, Feluy, B-7181 Seneffe, Belgium

Supporting Information Placeholder

ABSTRACT: The engineering of RHO nanozeolite is demonstrated by synthesis from a colloidal precursor suspension using inorganic structure-directing agents only (Na^+, Cs^+) whereby the particle morphology, Si/Al ratio, cation content, stability and flexibilty are tailored. RHO nanozeolite with a higher Si/Al ratio (2.0) and superior thermal stability (up to 700 °C) compared to previous reports is synthesized. Optimization of the synthesis procedure by introducing additional Si precursors facilitated the targeted improvement in the Si/Al ratio while maintaining the nano-sized dimensions of the discrete zeolite crystals with well-defined rhombic dodecahedral morphology. The structural properties of the RHO nanosized zeolites are characterized by in situ variable temperature XRPD experiments showing that the nanozeolite possesses a single structural phase up to 740 °C; further heating to 760 °C induces a symmetry change from noncentrosymmetric to centrosymmetric associated with a large increase in the anisotropic displacement parameter of the Cs^+ extra-framework cations. The structural behavior is unique compared to more silicious Na^+ and Cs^+ containing RHO zeolites (Si/Al ≥ 3) which possess centrosymmetric structure when hydrated. These experiments reveal a delineation, based on the Si/Al ratio and content of the extra-framework cations, between as-synthesized Na^+ and Cs^+ containing RHO zeolites that possess centrosymmetric or noncentrosymmetric symmetry when hydrated as well as single or co-existing structural phases, expanding the scope of intelligently designed nanozeolites with tailored properties for precise applications.

Keywords: zeolites, flexibility, stability, cations, nanomaterials, adsorption

■ INTRODUCTION

Zeolites are microporous crystalline solids that play key roles in petrochemistry and consumer products, as well as possessing significant potential in biomedical applications.[1-3] Their regular micropore networks allow for the selective adsorption and separation of molecules, providing size and shape selective environments for acid and base catalysed reactions. Nanozeolites offer several key advantages over conventional micron-sized zeolites such as a greater number of accessible active sites, more rapid diffusion of guest molecules, and a greater number of external silanol defects which can be utilised for zeolite engineering.[4-6] However, only 25 of the 255 IZA registered frameworks have been prepared as nanozeolites and many syntheses involve the use of organic structure-directing agents (OSDAs) which are expensive and require a destructive removal by calcination generating NO_x and CO_x emissions. This last point, while often overlooked in academia, presents critical challenges during scaling-up as this highly exothermic process in the presence of H_2O vapour can dramatically change the zeolite properties (*e.g.* framework Si/Al, porosity) and related performances. To address this we have developed synthetic strategies to prepare nanozeolites using inorganic structure-directing agents only.[7-11] However, understanding the crystallisation pathway of nanozeolites in order to target a specific framework topology and finely tune their properties including particle size, morphology, Si/Al ratio, and cation content through a direct synthesis approach remains a grand challenge of synthetic chemistry.[12]

Recently, we reported the first synthesis of flexible RHO nanozeolite from a colloidal precursor mixture using inorganic structure-directing agents only.[9, 13] The high-aluminum containing (Si/Al = 1.4–1.5) RHO nanozeolite exhibited high selectivity for CO_2 adsorption over CH_4, however, the CO_2 adsorption capacity was low due to the high extra-framework cation content. Laboratory *in situ* variable temperature X-ray powder diffraction (XRPD) and synchrotron measurements revealed the RHO nanozeolite possesses two co-existing structural phases. The structural properties of each phase are dependent on its chemical composition in addition to changes in temperature and the type of adsorbed molecules (H_2O, CO_2). Since its discovery RHO zeolite has attracted interest due to its remarkable and complex structural flexibility;[14-15] undergoing significant and reversible transformations in response to changes in the extra-framework cation content,[16-20] temperature,[21] pressure,[22-23] and guest molecule chemistry.[24-29] Specifically, H_2O plays a key role in defining the coordination environment of extra-framework cations and thus the sym-

metry adopted by the framework.[25, 30] The RHO structure is described by truncated cuboctahedra (*lta* cages) linked by double eight-membered rings (D8Rs) creating two interpenetrating but not interconnected pore systems. As-synthesised RHO zeolite contains both Na^+ and Cs^+ extra-framework cations; the latter serves to direct the crystallisation of the RHO framework, however, Cs^+ can be substituted by a cationic OSDA.[31] Depending on their properties, extra-framework cations may occupy three different positions within the RHO framework: at the D8Rs, at the single eight-membered rings (S8Rs), or at the single six-membered rings (S6Rs) within the *lta* cage. The flexible behaviour of RHO zeolite is described by the ability of the structure to change between the cubic centrosymmetric *Im*-3*m* and noncentrosymmetric *I*-43*m* space groups, corresponding to a tetrahedral distortion of the *lta* cages and change in the shape of the D8Rs from round to elliptical. The distortion or ellipticity (Δ) of the D8Rs can be described by the average of the shortest and longest O–O distances within the cross-section of the D8R.[32] The ability to easily tune the pore size and shape by simply varying the extra-framework cation content allows for the facile tuning of the zeolite's properties for applications such as catalysis and adsorption.[27, 33-36] In particular, due to the ability of zeolite RHO to selectively adsorb CO_2 over non-polar molecules such as CH_4 and N_2, the last decade has seen renewed investigation and further characterisation of the structural behaviour of RHO focussing on the extra-framework cation content and adsorption performance of the zeolite.[27-28, 30, 37-44]

Here we report on the synthesis of RHO nanozeolite with Na^+ and Cs^+ inorganic structural directing agents to obtain a product with an increased Si/Al ratio of 2 (referred to as Na,Cs-RHO-2.0) and improved thermal stability up to 700 °C compared to previous efforts. Judicious optimization of the synthesis parameters (alkali metal and water content, ageing, Si source) allowed for increasing of the Si/Al ratio while maintaining the nano-sized dimensions of the discrete zeolite crystals which possess well-defined morphology. In particular, ageing plays a critical role as it was found that ageing of the colloidal precursor at room temperature for 21 days produced crystalline nanozeolite RHO, similar to the synthesis protocol of BPH nanosheets.[11] *In situ* variable temperature XRPD analysis reveals that the new nanozeolite (Na,Cs-RHO-2.0) possesses a single crystalline phase (*I*-43*m*) at temperatures between 30 and 740 °C, in contrast to other nanozeolite RHO samples, demonstrating that the framework aluminum content and loading of extra-framework cations can be tuned in order to precisely control the flexible behavior of as-synthesized Na,Cs-RHO zeolite. Surprisingly, analysis of the nanozeolite from 700 to 800 °C revealed a symmetry change from noncentrosymmetric to centrosymmetric space group between 740 and 760 °C, behavior which had previously only been observed for deuterium-exchanged deammoniated RHO (D-RHO) and Cd-RHO at lower temperatures. This symmetry change is related to the significant displacement of the Cs^+ extra-framework cations through the D8Rs.

■ EXPERIMENTAL

Synthesis. LUDOX® AS-40 colloidal silica (SiO_2, Aldrich, 40 wt% suspension), sodium aluminate ($NaAlO_2$, 50–56% Al_2O_3, 40–45% Na_2O Sigma-Aldrich) and sodium hydroxide (NaOH, VWR Chemicals, 99%) were used as received. An aqueous solution of caesium hydroxide (CsOH, 50 wt% Cs) was prepared by dissolving caesium hydroxide (Alfa Aesar 20% H_2O, 98%) in de-ionised water. All water used was double distilled using an Aquatron water still A4000D.

The samples of nanozeolite RHO presented in this work are listed in Table 1. The synthesis of the RHO nanozeolite (Na,Cs-RHO-2.0) was performed in a sealed 60 mL polypropylene bottle. Sodium aluminate (0.518 g) was dissolved in de-ionised water (2.12 g) with rapid stirring, followed by the addition of sodium hydroxide (1.78 g) and aqueous caesium hydroxide (0.388 g). After 1 h of stirring at room temperature the alkali aluminate solution was heated statically at 60 °C for 30 min followed by cooling to room temperature with rapid stirring for 30 min. Colloidal silica (4.77 g) was then added dropwise with rapid stirring. The alkali aluminosilicate colloidal suspension was then aged with rapid stirring for 2 days. The molar ratio of oxides of the initial alkali aluminosilicate colloidal suspension was $0.23Cs_2O•8.08Na_2O•10SiO_2•0.8Al_2O_3•90H_2O$. Extra colloidal silica (3.81 g) was then added, immediately followed by a mixture of sodium silicate (1.855 g) and sodium hydroxide (0.27 g), both dropwise and with rapid stirring. The final alkali aluminosilicate colloidal suspension was stirred for a further 24 h before static hydrothermal treatment in a preheated oven at 90 °C for 2 h. The final molar ratio of oxides was $0.23Cs_2O•10.12Na_2O•20.6SiO_2•0.8Al_2O_3•150.4H_2O$. The recovered material was washed with hot (90 °C) de-ionised water by centrifugation until the pH of the supernatant was 7–8. The washed nanozeolite was then dried at 60 °C overnight. RHO nanozeolite synthesised at room temperature (Na,Cs-RHO-RT-21D) was prepared, washed and dried in almost identical fashion to Na,Cs-RHO-2.0 using an initial alkali aluminosilicate colloidal suspension of $0.30Cs_2O•8.08Na_2O•10SiO_2•0.8Al_2O_3•120H_2O$. After addition of the colloidal silica the mixture was rapidly stirred at room temperature for 21 days before washing by centrifugation and drying. Calcination experiments in air were performed at 700 °C for 12 h and 900 °C for 2 h. Samples were heated at 5 °C min^{-1} to 120 °C and held for 1 h, followed by heating at 5 °C min^{-1} to 250 °C and held for 1 h, and finally heated at 5 °C min^{-1} to the target temperature.

Table 1. Sample name and synthesis composition of nanzeolite RHO presented in this work.

Sample	Synthesis Composition
Na,Cs-RHO-2.0	$0.23Cs_2O•10.12Na_2O•20.6SiO_2•0.8Al_2O_3•150.4H_2O$
Na,Cs-RHO-RT-21D	$0.30Cs_2O•8.08Na_2O•10SiO_2•0.8Al_2O_3•120H_2O$

Characterization. X-ray powder diffraction (XRPD) patterns were collected with a PANalytical X'Pert Pro diffractometer using Cu Kα1 radiation (λ = 1.5406 Å, 45 kV, 40 mA). The patterns were collected between 5–60° 2θ with a step size of ~0.0167° and time per step of 1000 s.

Variable temperature X-ray powder diffraction data was collected on a Rigaku SmartLab diffractometer using a rotating anode (Cu Kα radiation, λ = 1.54 Å, 45 kV, 200 mA) and an Anton Paar HTK1200N high-temperature chamber. The XRPD pattern were collected in Bragg-Brentano configuration with a HyPix-3000 detector from 7–100° 2θ with a step size of 0.01° and a measurement speed of 1.5° min^{-1}. Variable temperature XRPD data was collected between 30 °C and 800 °C under air with a heating rate of 5 °C min^{-1}. Structural analysis (Rietveld refinements) was performed using the program JANA2006 and JANA2020.[45]

High-Resolution Transmission Electron Microscopy (HRTEM) imaging was performed with a FEI Tecnai G2 30 microscope

(V_{acc} = 300 kV, LaB_6). The particles of the as-synthesised samples were diluted in absolute ethanol, then the suspension was deposited and dried on carbon-film covered copper grids.

^{29}Si and ^{27}Al magic-angle spinning (MAS) NMR experiments are performed at 99.3 and 130.3 MHz respectively on a 500 MHz (11.7 T) Bruker Avance III-HD spectrometer using a 4 mm probe head, the sample is rotated at a spinning rate of 12 kHz. The chemical shifts are referenced to tetramethyl silane (TMS) and $AlCl_3$ respectively. Radio frequency (rf) field strength of 36 and 50 kHz and recycle delays of 20 and 1 second were used respectively. 10240 and 725 scans were collected for each nucleus respectively.

Inductively coupled plasma mass spectrometry (ICP-MS) measurements were recorded using a 7900 ICP-MS from Agilent Technologies.

N_2 adsorption/desorption isotherms were measured at -196 °C and the CO_2 adsorption isotherm was measured at 0 °C using a Micromeritics 3Flex Surface Characterisation unit. Samples were degassed at 350 °C under vacuum for 8 h prior to analysis.

Thermogravimetric analysis (TG/DTG) was performed using a TAG24 SETARAM analyser under N_2 atmosphere. Measurements were performed between 30 and 1000 °C with a ramp rate of 1 °C min^{-1}.

Simultaneous Differential scanning calorimetry (DSC) data and TG data was acquired with a NETZSCH STA 449F3 instrument under flowing N_2. The sample was heating from 30 °C to 800 °C with a heating rate of 2 °C min^{-1}.

■ RESULTS AND DISCUSSION

Synthesis Strategy

The synthesis engineering of nanozeolite RHO was developed to achieve two goals: (1) to increase the Si/Al ratio (simultaneous decrease of the extra-framework cation content), and (2) to maintain the nano-sized dimensions of the zeolite crystals. Typically, the preparation of nanozeolites from clear solutions without the use of OSDAs requires a high concentration of alkali metal cations to solubilise Si and maintain the high pH necessary to stabilise the aluminosilicate colloidal suspension.[7] However, this produces nanozeolites with a high aluminum and extra-framework cation content which may result in a low adsorption capacity for certain types of zeolites depending on the framework topology. In order to address the low adsorption capacity of the RHO nanozeolite the Cs content of the synthesis mixture was reduced. Reduction of the Cs content must be carefully controlled because Cs^+ cations play a critical role during the synthesis process whereby they substitute Na^+ cations in the amorphous aluminosilicate particles, promoting long-range crystalline order and facilitating the crystallisation of the zeolite framework.[11, 46]

Following our RHO nanozeolite synthesis reported earlier, the preparation of Na,Cs-RHO-2.0 nanozeolite began with an alkali aluminosilicate colloidal suspension composed of sodium aluminate, de-ionised water, sodium and caesium hydroxides, and colloidal silica aged at room temperature with rapid stirring (Figure 1). In order to increase the Si/Al ratio of the RHO nanozeolite a staged addition of Si species to the alkali aluminosilicate colloidal suspension was performed (Figures 1b–e). This strategy was adapted from the synthesis of nano-sized chabazite whereby a Si/Al ratio of 2 was achieved by increasing the content of colloidal silica during the ageing step.[10] The addition of Si involved a mixture of colloidal and molecular Si species in the presence of sodium hydroxide to promote solubility. The presence of the additional Na^+ cations is also critical for facilitating the polymerization of the Si and crystallization of the zeolite without requiring an increase in the time of hydrothermal treatment which promotes particle growth (Figure. S1, Table S1). The addition of the extra Si also increases the H_2O content of the synthesis mixture. This necessitates that the H_2O content of the initial mixture be decreased in order to minimize the particle growth at the expense of nucleation during the hydrothermal treatment. Finally, precise control of the ageing of the alkali aluminosilicate colloidal suspension was necessary to facilitate crystallization of the zeolite framework during the hydrothermal treatment after addition of the extra Si. Without the addition of extra Si, ageing of the alkali aluminosilicate colloidal suspension with rapid stirring for 21 days affords crystalline RHO nanozeolite at room temperature (Na,Cs-RHO-RT-21D), similar to BPH nanosheets (Figure S2).[11] Based on our previous work, this indicates that at a specific time during the ageing step the dominant process of the system changes from nucleation to crystallisation.[11, 46] For the synthesis of

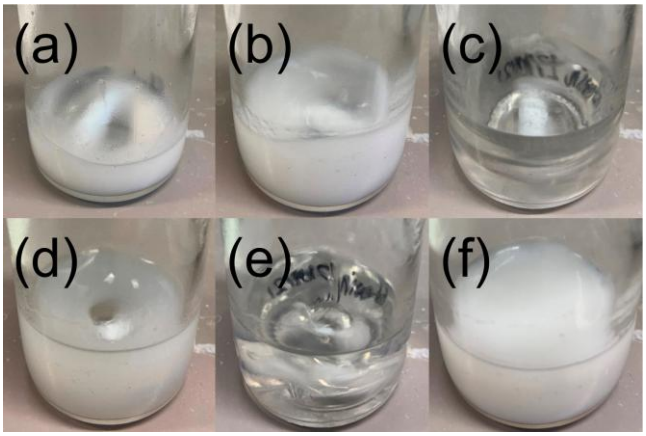

Figure 1. Evolution of the synthesis precursor mixture: (a) alkali aluminate mixture of metal hydroxides, (b) alkali aluminosilicate colloidal suspension immediately after the first addition of Si, (c) alkali aluminosilicate colloidal suspension becomes clear after 7 h of ageing, (d) alkali aluminosilicate colloidal suspension immediately after the second addition of Si, (e) alkali aluminosilicate colloidal suspension after 1 day of ageing since second addition of Si, (f) alkali aluminosilicate colloidal suspension after hydrothermal treatment for 2 h at 90 °C.

Na,Cs-RHO-2.0, the addition of extra Si was performed after 2 days of rapid stirring; if added earlier the RHO framework does not crystallize within the 2 h of hydrothermal treatment at 90 °C, and reflections attributable to FAU are observed (Figure S1, Table S1). This indicates that insufficient formation of amorphous (when analyzed by XRPD) aluminosilicate nucleates with short range crystalline order has occurred, as well as insufficient distribution of Cs^+ cations throughout the mixture.[47] After the addition of the extra Si, the alkali aluminosilicate colloidal suspension was aged under stirring for a further 24 h to allow for solubilization of the extra Si before the hydrothermal treatment.

Characterization of RHO Nanozeolite

XRPD data analysis of the as-synthesised hydrated Na,Cs-RHO-2.0 sample allowed the determination of one crystalline phase of RHO (Figure 2); no reflections attributable to FAU

were observed despite the relatively low Cs^+ content.[47-48] Rietveld refinement of the XRPD pattern recorded at 30 °C was performed using the space group *I*-43*m*; the lattice parameter *a* was calculated to be 14.7570(8) Å and the reliability factors were GOF = 1.91 and R_{wp} 5.12%. The lattice parameter of the as-synthesised hydrated Na,Cs-RHO-2.0 sample is smaller than that previously reported for as-synthesised OSDA-free hydrated RHO nanozeolites which possess a higher Al content and structure with the *I*-43m space group (Table S2). This is consistent with the differences in the Si/Al ratio and the Si–O and Al–O bond lengths. Elemental analysis by inductively-coupled plasma mass spectroscopy and energy dispersive X-ray analysis combined with thermogravimetric analysis (TGA) gave the following compositions of Na,Cs-RHO-2.0, $(Na_{11.6}Cs_{5.0})Si_{31.4}Al_{16.6}O_{96}\bullet 37H_2O$ (Si/Al = 1.9) and $(Na_{11.0}Cs_{5.1})Si_{31.9}Al_{16.1}O_{96}\bullet 37H_2O$ (Si/Al = 2.0) respectively. The calculated yield derived from the dry mass of the product against the dry mass of starting SiO_2 and Al_2O_3 was 26% due to the two-fold increase of SiO_2 content in the synthesis colloidal suspension compared to previously reported syntheses. The amount of Cs incorporated into the product from the synthesis colloidal suspension was similar to the conventional OSDA-free synthesis (74 *vs* 80% Cs)[14] and higher than that of the OSDA route (16.4 *vs* 10.6 wt% Cs_2O).[49] The content of Al, Si and Na in the product were 72, 11 and 0.5% respectively, making the synthesis supernatant a prime candidate for recycling studies. Compared to our previous RHO nanozeolite syntheses the Cs necessary to obtain crystalline RHO in this experiment was halved.

^{29}Si MAS NMR spectroscopic analysis of the Na,Cs-RHO-2.0 sample identified five resonances assigned to $Q^0(4Al)$, $Q^1(3Al)$, $Q^2(2Al)$, $Q^3(1Al)$, and $Q^4(0Al)$ species at −84.5, −88.5, −93.1, −97.8, and −103.0 ppm, respectively (Figure 3a). Deconvolution of the ^{29}Si MAS NMR spectrum and using the Engelhardt equation, the Si/Al ratio was calculated to be 2.1. ^{27}Al MAS NMR spectroscopy revealed a single resonance at 62 ppm; no signal corresponding to extra-framework aluminum was observed (Figure 3b).

High-resolution transmission electron microscopy (HRTEM) of Na,Cs-RHO-2.0 sample revealed the presence of well-defined nanocrystals with rhombic dodecahedral morphology (Figure 4). Particle counting identified the size of the nanocrystals to vary approximately between 50 to 100 nm depending on the crystal orientation (Figure S3). Two maxima were identified at approximately 60 and 85 nm consistent with the geometric properties and morphology of the crystals; the length of the long-faced diagonal is the product of $\sqrt{2}$ and the short-face diagonal. Compared to the previously reported RHO nanozeolite and Na,Cs-RHO-RT-21D, Na,Cs-RHO-2.0 possesses sharper crystal facets and well-defined morphology (Figure S4). This can be due to the complete crystallization of the nanoparticles due to the increased time of hydrothermal treatment and increased concentration of Si available in the colloidal suspension.

N_2 sorption analysis showed the Na,Cs-RHO-2.0 sample exhibits negligible uptake of N_2 in the low (< 0.1 P/P_0) relative pressure region (Figure 5a). This is attributed to the "trapdoor" mechanism where zeolites possessing eight-membered rings (8R) (*e.g.* RHO, CHA) occupied by extra-framework cations selectively adsorb small molecules (*e.g.* CO_2) depending on the molecule-cation

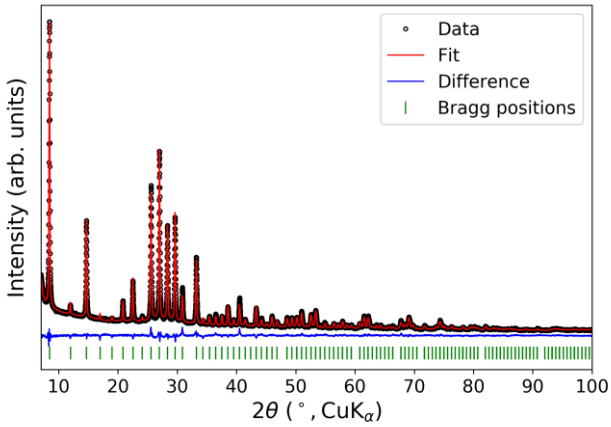

Figure 2. Results of the Rietveld refinements of the XRPD data of the as-synthesized Na,Cs-RHO-2.0 nanozeolite measured at 30 °C.

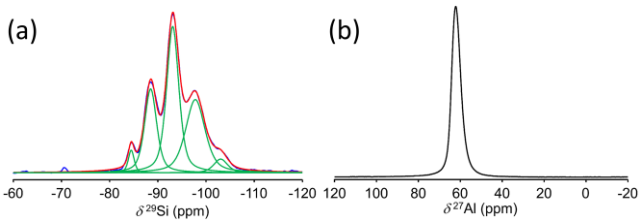

Figure 3. (a) ^{29}Si and (b) ^{27}Al MAS NMR spectra of the as-synthesized Na,Cs-RHO-2.0 nanozeolite.

interaction and thermal oscillation of the cation at a specific temperature.[50-54] At 77 K N_2 is unable to enter the RHO micropores due to the blocking of the 8Rs by Cs^+ extra-framework cations. At high relative pressure (> 0.85 P/P_0) the quantity of adsorbed N_2 notably increases due to the inter-particle mesoporosity of the nanozeolite; similar behavior is observed for Na,Cs-RHO-RT-21D (Figure S5). CO_2 adsorption analysis at 273 K showed improved capacity and uptake by Na,Cs-RHO-2.0 in the low pressure region compared to the previously reported RHO nanozeolite (Figure 5b).[9] This is due to the reduction of the Cs^+ content from 6 to 5 cations per unit cell and lower ellipticity upon dehydration (*vide infra*) allowing for less restricted access of CO_2 to the RHO cage, as well as the reduction of the Na^+ content from 13 to 12 cations per unit cell (based on ICP-MS).

Variable temperature structural analysis of Na,Cs-RHO-2.0 to 700 °C

The stability and structural properties of the Na,Cs-RHO-2.0 sample were investigated by *in situ* variable temperature XRPD up to 700 °C in air; the scans are presented in Figure. 6. During

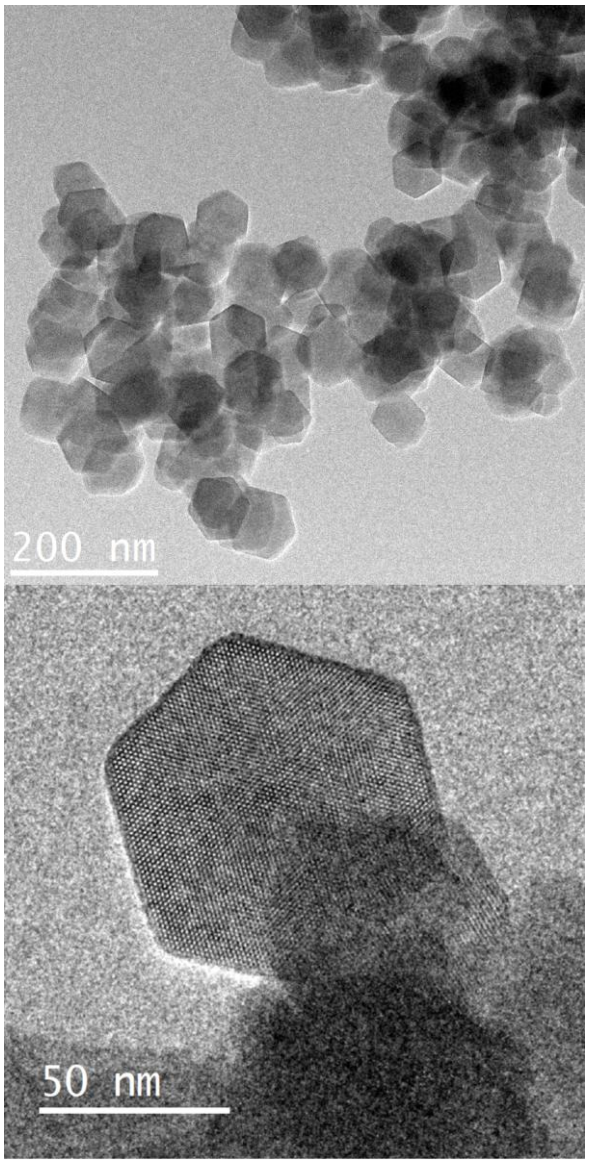

Figure 4. HRTEM images of the as-synthesized Na,Cs-RHO-2.0 nanozeolite.

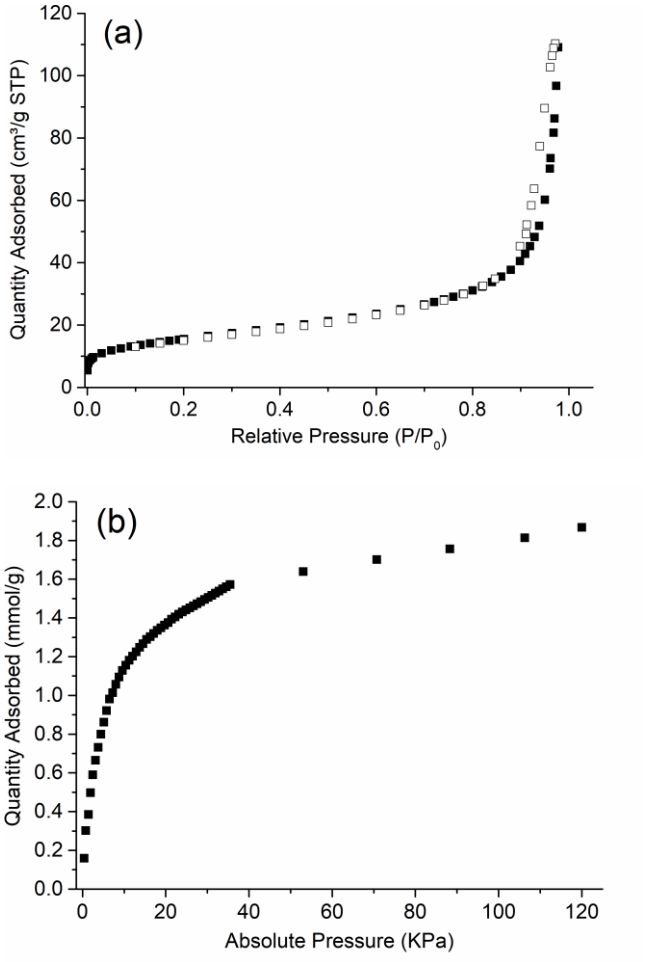

Figure 5. (a) N_2 adsorption (filled) and desorption (empty) isotherms measured at 77 K and (b) CO_2 adsorption isotherm measured at 273 K of the as-synthesized Na,Cs-RHO-2.0 nanozeolite.

the structural refinements, the water content in the structures were fixed to the values determined from thermogravimetric (TG) analysis (Figure S6) and used up to a temperature of 300 °C. Due to the high water content and the lack of a high-resolution instrumental set-up (*e.g.* monochromatic radiation), a higher degree of uncertainty was associated with locating the water molecules and the lighter Na^+ ions in the structure. The crystallographic parameters (lattice parameter, atomic positions, and atomic displacement parameters) of the Na,Cs-RHO-2.0 sample heated at different temperatures were determined by Rietveld refinements (Figures 2, S7, S8, Tables S4–22). As stated earlier, *a* of the as-synthesized hydrated Na,Cs-RHO-2.0 sample at 30 °C was determined as 14.7570(8) Å with *I*-43*m* space group, consistent with its higher Si/Al ratio compared to previously reported Na,Cs-RHO nanozeolites. However, this value is smaller compared to that of hydrated conventional micron-sized Na,Cs-RHO zeolite (Si/Al = 3–4) synthesized with or without OSDAs, with $a \approx 15.0$ Å and *Im*-3*m* space group (Table S3).[14, 55-56] Partial dehydration of micron-sized Na,Cs-RHO at 100 °C results in a contraction of *a* (14.6566(4), 14.678(1) Å) and a change of space group to *I*-43*m* as reported by Baur *et al.*, and McCusker and Baerlocher respectively (Table S3).[55, 57] These values are slightly smaller than the value of 14.6867 Å determined for Na,Cs-RHO-2.0 partially dehydrated at 90 °C, consistent with its lower Si content and greater number of extra-framework

cations. The larger value of *a* and *Im*-3*m* space group for the hydrated micron-sized RHO zeolite is due to the different number and location of extra-framework cations, specifically the occupation of the S8Rs by Cs^+ (Table S3). For hydrated micron-sized RHO measured at room temperature the Cs^+ cations are located slightly off the plane of the S8Rs, while Na^+ cations are identified near the plane of the S6R in the *lta* cages, off-center of the 8MRs, and within the D8Rs.[55-56] The adoption of the *Im*-3*m* space group for hydrated micron-sized RHO is consistent with the structural results of Palomino *et al*. and Lozinska *et al*. whereby the adsorption of CO_2 at 100 kPa by either dehydrated Na,Cs-RHO or Cs-RHO initiates a symmetry change from noncentrosymmetric to centrosymmetric.[27, 39] This change is related to the displacement of Cs^+ from the D8Rs to the S8Rs, reducing the distortion of the 8Rs. The rapid contraction of the lattice parameter and change of symmetry from centrosymmetric to noncentrosymmetric of micron-sized Na,Cs-RHO upon dehydration from room temperature to 100 °C is due to the relocation of Cs^+ extra-framework cations from the S8Rs to the D8Rs. Similar behavior has also been observed for Cs,Ca-, Pb- and Cd-RHO with a Si/Al = 3.1.[18, 25]

In comparison, for the hydrated Na,Cs-RHO-2.0 sample measured at 30 °C, Cs^+ cations occupy the center of the D8Rs while Na^+ cations partially occupy positions near the plane of the S6Rs in the *lta* cages; no H_2O molecules were located within the D8Rs consistent with previous reports (Figure 7).[56-57] As the temperature of the Na,Cs-RHO-2.0 nanozeolite is increased different behavior is identified related to changes in the lattice parameter,

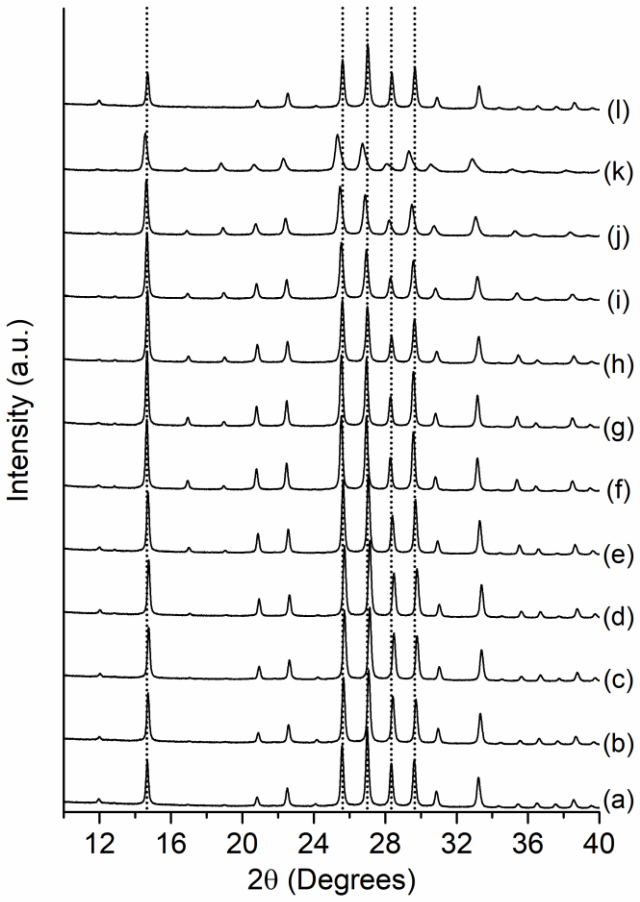

Figure 6. *In situ* variable temperature XRPD scans of Na,Cs-RHO-2.0 from 30 to 700 °C and back to 28 °C: (a) 30 °C, (b) 60 °C, (c) 90 °C, (d) 120 °C (e) 150 °C, (f) 200 °C, (g) 300 °C, (h) 400 °C, (i) 500 °C, (j) 600 °C, (k) 700 °C, (l) 28 °C. Dotted lines guide the eye to highlight the shift in the position of the reflections as a function of temperature.

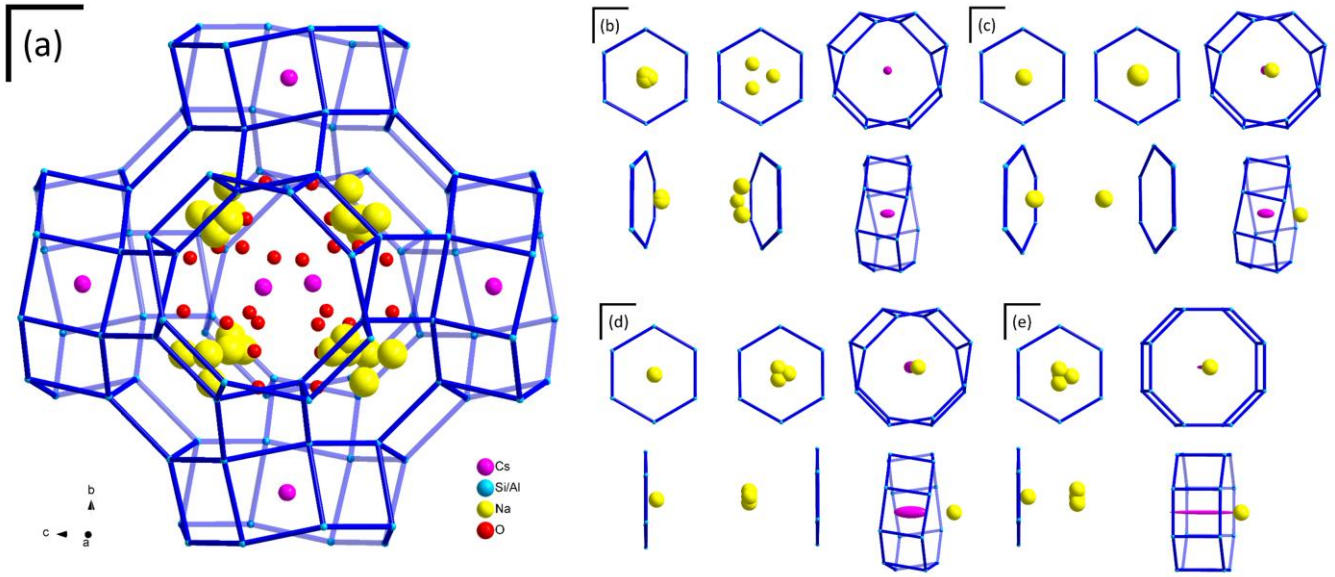

Figure 7. (a) Framework structure, extra-framework cations, and oxygen atoms of H_2O molecules of the as-synthesized Na,Cs-RHO-2.0 nanozeolite obtained from Rietveld analysis of data recorded at 30 °C. (b-e) S6R and 8DR structures and extra-framework cations at (b) 150 °C, (c) 200 °C, (d) 700 °C and (e) 800 °C. The anisotropic atomic displacement parameters for the Cs^+ extra-framework cations are shown.

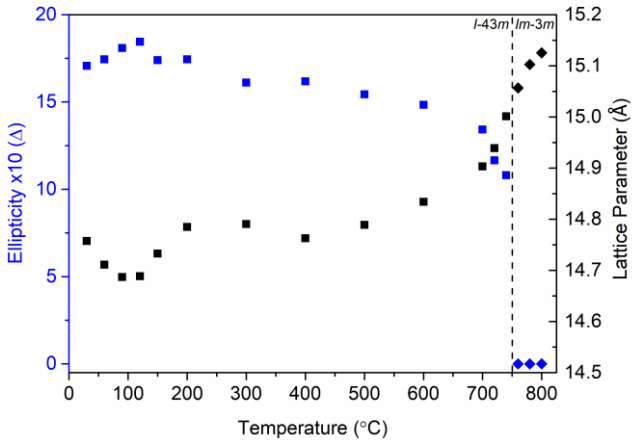

Figure 8. Plot of the ellipticity ×10 of the D8Rs (blue) and the lattice parameter (black) of the as-synthesized Na,Cs-RHO-2.0 nanozeolite as a function of temperature in air. The line delineates the adoption of either the noncentrosymmetric (squares) or centrosymmetric (diamonds) space group as a function of temperature.

ellipticity (Figure 8) and Na^+ cation locations (Figure 7). In comparison to the Na^+, the Cs^+ extra-framework cations do not move from their average positions within the D8Rs between 30 and 800 °C. However, a higher level of mobility is observed at elevated temperatures represented by the increase of the U_{11} atomic displacement parameter for Cs^+ above 600 °C (Table S7–S22, Figure S9). From 30 to 120 °C an initial decrease in the lattice parameter to 14.6885(2) Å is observed while the ellipticity of 8MRs increases from to 1.72 to 1.85. This is attributed to the removal of water molecules from the *lta* cage and the initial movement of Na^+ cations closer to the plane of the S6Rs. Calculated from TG analysis, the number of H_2O molecules per unit cell decreases from 37 to 22. Heating from 120 to 200 °C the lattice parameter increases to 14.7847(8) Å; from 150 to 200 °C the locations of the Na^+ cations change and the number of H_2O molecules per unit cell decreases from 14 to 6. The ellipticity of the 8MRs remains approximately constant from 150 to 200 °C before decreasing non-linearly to 1.34 at 700 °C. A similar trend has previously been observed for D-RHO.[21] The lattice parameter remains approximately constant from 200 to 300 °C before decreasing slightly at 400 °C. Above 400 °C it begins to increase non-linearly, reaching 14.9033 Å at 700 °C, following the complete removal of water from the structure (Figure S6). Above 200 °C the Na^+ cations fully occupy one position near the plane of the S6Rs (Na1), as well as partially occupy a second position slightly off-center of the S8Rs (Na2) and a third position between the center of the *lta* cage and S6R (Na3). As the temperature increases to 700 °C the Na^+ cations located at the S8R displace slightly towards the center of the *lta* cage while the Na^+ cations near the plane of the S6Rs do not significantly change their average position, and the residual Na^+ at the third position displaces closer to the center of the *lta* cage. Due to the partial occupancy of the Na^+ at the S8R and Cs^+ at the D8R positions, one may imagine on average that for the 8R pore apertures all of the five Cs^+ cations are located within a D8R while one Na^+ is located off-center of a S8R. The position and intensity of the reflections in the XRPD pattern changed slightly from the start and after the complete removal of water (60–300 °C) from the sample; from 400 to 700 °C a slight shift to lower values of °2θ is observed. Cooling the sample from 700 °C back to room temperature in air showed the structural changes to be completely reversible (a = 14.7364(4) after heating) due to the re-adsorption of H_2O, with negligible change to the crystallinity of the sample (Figure S10).[25] The stability of the Na,Cs-RHO-2.0 sample was tested further by calcination in air at 700 °C for 12 h revealing the structure to be stable (Figure S11). Analysis by ^{27}Al MAS NMR spectroscopy showed no extra-framework aluminum was formed, however, the shape of the resonance indicated the formation of disordered tetrahedrally-coordinated Al (Figure S12).

Interestingly, the *in situ* variable temperature XRPD analysis of Na,Cs-RHO-2.0 did not lead to any splitting of the reflections as was observed for other RHO nanozeolite samples.[9, 13] This shows that the Na,Cs-RHO-2.0 sample does not exhibit

any behavior indicating the presence of two co-existing crystalline phases as a function of temperature and hydration. This is attributed to its higher Si/Al ratio and lower extra-framework cation content. For as-synthesized Na,Cs-RHO zeolites, this behavior has only been observed for nanozeolite samples with a Si/Al content < 2.[9, 13] For zeolite RHO, this phenomenon is controlled by the loading of guest molecules (H_2O, CO_2) as well as the type, number and location of extra-framework cations. Co-existing crystalline phases have been observed for hydrated micron-sized RHO with a Si/Al ≈ 3, such as Ca,NH_4/ND_4-RHO, due to the difference in the size and charge density between Ca^{2+} and NH_4^+ located at the D8Rs.[18] Recently, micron-sized Na,Cs- and Cs-RHO (Si/Al ≈ 4) were reported to exhibit co-existing crystalline phases in the presence of 5% humidity.[29] The delivery of CO_2 at different pressures to dehydrated micron- and nano-sized RHO also induces the co-existence to two crystalline phases due to the displacement of the extra-framework cations in the presence of CO_2.[13, 27, 39, 41] This behavior has also been observed for Na-RHO in the co-presence of both H_2O and CO_2.[29] In the case of as-synthesized Na,Cs-RHO with similar water content, the number of extra-framework cations as a function of the Si/Al ratio is the primary factor for the co-existence of two crystalline phases under ambient (hydrated) conditions. As the Si/Al ratio increases from 1.5 to 1.7 and the loading of extra-framework cations decreases, heating/dehydration of the Na,Cs-RHO is necessary to induce this phenomena.[13]

High-temperature symmetry change of Na,Cs-RHO-2.0

Further heating of the Na,Cs-RHO-2.0 sample up to 800 °C revealed a distinct shift in the position and intensity of the reflections in the XRPD pattern indicative of a change in symmetry (Figures 9, 10). To identify more clearly the temperature at which the symmetry change occurred the sample was measured from 700 to 800 °C at 20 °C intervals; after each scan at high temperature the sample was cooled and measured at room temperature. Calculation of the lattice parameter revealed a new region of structural behaviour; from 700 to 780 °C the lattice parameter increased sharply from 14.9033 to 15.1025 Å before approaching a plateau at 800 °C (Figure 8). Calculation of the ellipticity revealed a simultaneous rapid decrease; at 760 °C the ellipticity was found to be zero, suggesting the symmetry change occurs between 740 and 760 °C (Figure 9). Refinement of the structure using the space group *Im*-3*m* afforded the best fit values above 740 °C. The changes in the positions and intensities of the reflections are consistent with the change in symmetry from *I*-43*m* to *Im*-3*m* observed by Palomino *et al*.[27]

Analysis by differential scanning calorimetry (DSC) of the Na,Cs-RHO-2.0 sample illustrates further the occurrence of a gradual symmetry change at high temperature (Figure 11). A second order transition is observed commencing at approximately 740 °C. This second order transition is allowed by the space group change since *I*-43*m* is a subgroup of *Im*-3*m*. The absence of a sharp peak in the DSC curve indicates a gradual change; this is consistent with the gradual decrease in intensity of the XRPD reflections from 700 to 800 °C. However, the decrease in the intensity of the XRPD reflections may also be associated with the onset of amorphization (*vide infra*, Figure S13). The increase of the temperature from 700 to 800 °C and change in the space group from *I*-43*m* to *Im*-3*m* of Na,Cs-RHO-2.0 is associated with several changes in the cation locations: displacement of the Na^+ cations located next to the S6R closer to the S6R plane, movement of the Na^+ cations above the S8R closer to the S8R plane, and a major increase in the U_{11} atomic displacement parameter of Cs^+ cations in the D8R (Figure S9) such that they may no longer be considered located at a single position, but instead oscillating across the entire D8R structure, reaching the S8R position within the *lta* cage (Figure 9b). The small amount of residual Na^+ (Na3) remains near the center of the *lta* cage. Multiple cycles of heating and cooling of Na,Cs-RHO-2.0 between 30 and 800 °C showed reduced intensity

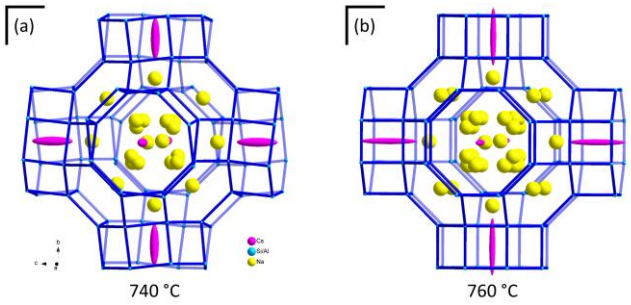

Figure 9. Framework structure and extra-framework cations of Na,Cs-RHO-2.0 nanozeolite obtained from Rietveld analysis of data recorded at (a) 740 °C and (b) 760 °C. The anisotropic atomic displacement parameters for the Cs^+ extra-framework cations are shown.

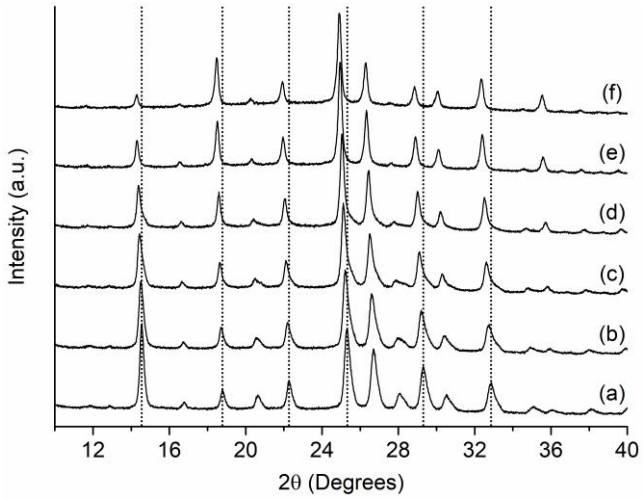

Figure 10. *In situ* variable temperature XRPD scans of Na,Cs-RHO-2.0 nanozeolite from 700 to 800 °C: (a) 700 °C, (b) 720 °C, (c) 740 °C, (d) 760 °C, (e) 780 °C, (f) 800 °C. Dotted lines guide the eye to highlight the shift in the position of the reflections as a function of temperature.

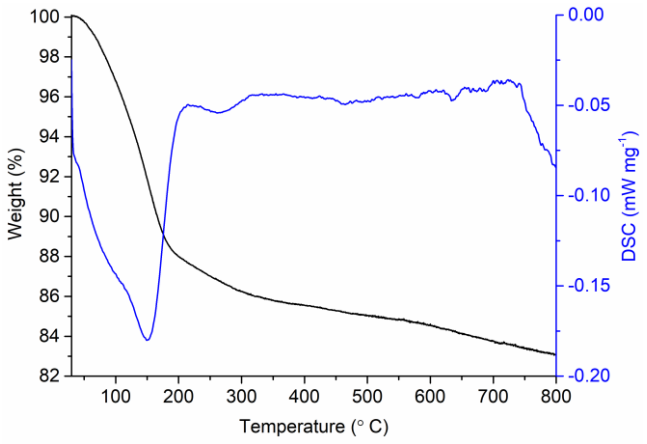

Figure 11. TG (black) and DSC (blue) curves of Na,Cs-RHO-2.0 nanozeolite from 30 to 800 °C.

of the pattern reflections indicating the structure was beginning to become amorphous (Figure S13). Calcination of the sample at 900°C resulted in the complete collapsed of the structure (Figure S11). The thermal stability of the Na,Cs-RHO-2.0 sample is 150 °C higher than our previously reported RHO nanozeolite and similar to recently reported thermochemistry results for micron-sized RHO zeolite, Si/Al = 3.2.[58] This shows that for Na,Cs-RHO the framework aluminum content is the determining factor of the thermal stability of the zeolite given the similar water content between Na,Cs-RHO-2.0 and previously reported Na,Cs-RHO nanozeolites.[9, 13]

In consideration with earlier studies on Pb- and Cd-RHO, these results shed further light on the complex structural flexibility of RHO zeolite as a function of temperature and the type, number, and location of extra-framework cations.[25] For Pb-RHO, dehydration of the structure up to 500 °C results in a non-linear contraction of the unit cell to ≈ 14.2 Å and noncentrosymmetric structure. The first stage is due to the removal of H_2O from the *lta* cage and the second due to the simultaneous removal of H_2O from the D8Rs and the shift of Pb^{2+} cations from the S8Rs to the D8Rs. In comparison, Cd-RHO displays more complex behavior similar to Na,Cs-RHO-2.0 where the unit cell initially contracts and then expands between 28 and 150 °C. This is followed by further contraction up to 450 °C due to Cd^{2+} cations moving from the S8Rs to the D8Rs as H_2O is removed. Above 450 °C a rapid expansion and the adoption of centrosymmetric structure occurs due to the relocation of Cd^{2+} cations to the S6Rs.

In the case of Na,Cs-RHO-2.0, all the S6Rs and nearly all the D8Rs are occupied at all times, however, increasing the temperature results in the displacement of Na^+ cations closer to the plane of the S6Rs and an enormous increase in displacement of the Cs^+ cations through the D8Rs. Despite the occupation of the S6Rs by Na^+, the temperature required to induce a symmetry change from noncentrosymmetric to centrosymmetric for Na,Cs-RHO-2.0 is significantly higher than that required for Cd-RHO due to the occupation and distortion of the D8Rs by Cs^+; the large oscillation of Cs^+ through the D8Rs and slightly into the *lta* cage at high temperature reduces the ability of the cation to interact and distort the 8R structure. This is supported by the observation that the changes of the U_{11} atomic displacement parameter of the Cs^+ extra-framework cations (Figure S9) and the lattice parameter of Na,Cs-RHO-2.0 (Figure 8) show near identical trends. This behaviour is further corroborated by the work of Palomino *et al*. and Lozinska *et al*. whereby the adsorption of CO_2 at 100 kPa by either NaCs-RHO or Cs-RHO initiates a symmetry change from noncentrosymmetric to centrosymmetric.[27, 39] This is associated with the displacement of Cs^+ from the D8Rs to S8Rs, reducing the distortion of the 8Rs. It is important to note that the presence of different cations being able to induce different symmetry in dehydrated RHO is a consequence of their size, charge density, and location. For example, Lozinska *et al*. observed noncentrosymmetric structure for dehydrated Li-RHO with 5.2 Li^+ at the S6Rs.[37] This is attributed to the significantly smaller size of Li^+ which requires strong distortion of the structure in order to achieve better coordination to the framework oxygens.

■ CONCLUSIONS

Through judicious optimization of the synthesis parameters, including cation content, ageing and hydrothermal treatment, we have demonstrated the engineered synthesis of Na,Cs-RHO nanozeolite with an improved Si/Al ratio (2.0) and thermal stability while maintaining discrete nanocrystal morphology. Ageing at room temperature of the alkali aluminosilicate suspension was found to play a critical role as RHO nanzeolite was found to crystallize at ambient conditions over 21 days. Reduction of the extra-framework Cs^+ cation content demonstrated improved uptake of CO_2 in the low pressure region. *In situ* variable temperature X-ray powder diffraction analysis up to 740 °C revealed the Na,Cs-RHO-2.0 sample possessed a single crystalline phase with the space group *I*-43*m* in contrast to other directly synthesized Na,Cs-RHO nanozeolites. This is due to its lower framework aluminum and extra-framework cation content. These results reveal a delineation for as-synthesized Na,Cs-RHO whereby two structural phases may coexist for a Si/Al ratio < 2. Heating of the Na,Cs-RHO-2.0 sample up to 760 °C revealed a change in symmetry from *I*-43*m* to *Im*-3*m* associated with the displacement of the Na^+ closer to the plane of S6R and a large oscillation of the Cs^+ through the D8R structure. Continued investigation of the RHO nanozeolite synthesis field to produce a higher Si/Al ratio for preparation of a stable H-form is ongoing.

ASSOCIATED CONTENT

Supporting Information

The Supporting Information is available free of charge on the ACS Publications website.

Contains characterization data including XRD patterns, synthesis and elemental compositions, TEM images, N_2 isotherms, TGA curve, ^{27}Al NMR spectra, and Rietveld refinement results including atomic positions, U_{iso} parameters and occupancies. (PDF)

AUTHOR INFORMATION

Corresponding Author

svetlana.mintova@ensicaen.fr

Notes

The authors declare no competing financial interests.

ACKNOWLEDGMENT

Financial support from TOTAL and Industrial Chair ANR-TOTAL “Nanoclean Energy” (Grant IPA 5621), the Label of Excellence for the Centre of Zeolites and Related Nanoporous

Materials by the Region of Normandy, as well as from the Normandy Region through the RIN Recherche Program (Grant 18P01675), and RIN Recherche DIXOS (Grant 18E01714/18P02440) is acknowledged.

REFERENCES

(1) Vermeiren, W.; Gilson, J.-P., Impact of Zeolites on the Petroleum and Petrochemical Industry. *Top. Catal.* **2009,** *52* (9), 1131-1161.

(2) Clatworthy, E. B.; Konnov, S. V.; Dubray, F.; Nesterenko, N.; Gilson, J. p.; Mintova, S., Emphasis on the properties of metal-containing zeolites operating outside the comfort zone of current heterogeneous catalytic reactions. *Angew. Chem.* **2020,** *132* (44), 19582-19600.

(3) Serati-Nouri, H.; Jafari, A.; Roshangar, L.; Dadashpour, M.; Pilehvar-Soltanahmadi, Y.; Zarghami, N., Biomedical applications of zeolite-based materials: A review. *Mater. Sci. Eng., C* **2020,** *116*, 111225.

(4) Mintova, S.; Gilson, J.-P.; Valtchev, V., Advances in nanosized zeolites. *Nanoscale* **2013,** *5* (15), 6693-6703.

(5) Mintova, S.; Grand, J.; Valtchev, V., Nanosized zeolites: quo vadis? *C. R. Chim.* **2016,** *19* (1-2), 183-191.

(6) Medeiros-Costa, I. C.; Dib, E.; Nesterenko, N.; Dath, J.-P.; Gilson, J.-P.; Mintova, S., Silanol defect engineering and healing in zeolites: opportunities to fine-tune their properties and performances. *Chem. Soc. Rev.* **2021,** *50* (19), 11156-11179.

(7) Ng, E.-P.; Chateigner, D.; Bein, T.; Valtchev, V.; Mintova, S., Capturing ultrasmall EMT zeolite from template-free systems. *Science* **2012,** *335* (6064), 70-73.

(8) Awala, H.; Gilson, J.-P.; Retoux, R.; Boullay, P.; Goupil, J.-M.; Valtchev, V.; Mintova, S., Template-free nanosized faujasite-type zeolites. *Nat. Mater.* **2015,** *14* (4), 447-451.

(9) Grand, J.; Barrier, N.; Debost, M.; Clatworthy, E. B.; Laine, F.; Boullay, P.; Nesterenko, N.; Dath, J.-P.; Gilson, J.-P.; Mintova, S., Flexible Template-Free RHO Nanosized Zeolite for Selective CO_2 Adsorption. *Chem. Mater.* **2020,** *32* (14), 5985-5993.

(10) Debost, M.; Klar, P. B.; Barrier, N.; Clatworthy, E. B.; Grand, J.; Lainé, F.; Brazda, P.; Palatinus, L.; Nesterenko, N.; Boullay, P.; Mintova, S., Synthesis of discrete CHA zeolite nanocrystals without organic templates for selective CO_2 capture. *Angew. Chem. Int. Ed.* **2020,** *59* (52), 23491-23495.

(11) Clatworthy, E. B.; Debost, M.; Barrier, N.; Gascoin, S. p.; Boullay, P.; Vicente, A. l.; Gilson, J.-P.; Dath, J.-P.; Nesterenko, N.; Mintova, S., Room-Temperature Synthesis of BPH Zeolite Nanosheets Free of Organic Template with Enhanced Stability for Gas Separations. *ACS Appl. Nano Mater* **2020,** *4* (1), 24-28.

(12) Awala, H.; Kunjir, S. M.; Vicente, A.; Gilson, J.-P.; Valtchev, V.; Seblani, H.; Retoux, R.; Lakiss, L.; Fernandez, C.; Bedard, R., Crystallization pathway from a highly viscous colloidal suspension to ultra-small FAU zeolite nanocrystals. *J. Mater. Chem. A* **2021,** *9* (32), 17492-17501.

(13) Confalonieri, G.; Grand, J.; Arletti, R.; Barrier, N.; Mintova, S., CO_2 adsorption in nanosized RHO zeolites with different chemical compositions and crystallite sizes. *Microporous Mesoporous Mater.* **2020,** *306*, 110394.

(14) Robson, H. E.; Shoemaker, D. P.; Ogilvie, R. A.; Manor, P. C., Synthesis and Crystal Structure of Zeolite Rho—A New Zeolite Retlated to Linde Type A. In *Molecular Sieves*, Meier, M. W.; Uytterhoeven, J. B., Eds. ACS Publications: Washington, D.C., 1973; Vol. 121, pp 106-115.

(15) Parise, J. B.; Liu, X.; Corbin, D. R., Flexibility of the zeolite RHO framework; relocation of cadmium accompanying transformation of the unit cell at high temperatures. *J. Chem. Soc., Chem. Commun.* **1991,** (3), 162-163.

(16) Flank, W., Properties of synthesized, ion-exchanged, and stabilized zeolite Rho. In *Molecular Sieves—II*, Katzer, J. R., Ed. ACS Publications: Washington, D.C., 1977; Vol. 40, pp 43-52.

(17) McCusker, L. B., Crystal structures of the ammonium and hydrogen forms of zeolite rho. *Zeolites* **1984,** *4* (1), 51-55.

(18) Corbin, D. R.; Abrams, L.; Jones, G.; Eddy, M.; Harrison, W.; Stucky, G.; Cox, D., Flexibility of the zeolite RHO framework: in situ x-ray and neutron powder structural characterization of divalent cation-exchanged zeolite RHO. *J. Am. Chem. Soc.* **1990,** *112* (12), 4821-4830.

(19) Bieniok, A.; Baur, W. H., A large volume contraction accompanies the low-to high-temperature phase transition of zeolite Sr-rho. *J. Solid State Chem.* **1991,** *90* (1), 173-177.

(20) Johnson, G. M.; Reisner, B. A.; Tripathi, A.; Corbin, D. R.; Toby, B. H.; Parise, J. B., Flexibility and cation distribution upon lithium exchange of aluminosilicate and aluminogermanate materials with the RHO topology. *Chem. Mater.* **1999,** *11* (10), 2780-2787.

(21) Parise, J. B.; Gier, T. E.; Corbin, D. R.; Abrams, L.; Jorgensen, J. D.; Prince, E., Flexibility of the framework of zeolite Rho. Structural variation from 11 to 573 K. A study using neutron powder diffraction data. *J. Phys. Chem.* **1984,** *88* (11), 2303-2307.

(22) Lee, Y.; Hriljac, J. A.; Vogt, T.; Parise, J. B.; Edmondson, M. J.; Anderson, P. A.; Corbin, D. R.; Nagai, T., Phase transition of zeolite RHO at high-pressure. *J. Am. Chem. Soc.* **2001,** *123* (34), 8418-8419.

(23) Nearchou, A.; Cornelius, M.-L. U.; Jones, Z. L.; Collings, I. E.; Wells, S. A.; Raithby, P. R.; Sartbaeva, A., Pressure-induced symmetry changes in body-centred cubic zeolites. *R. Soc. Open Sci.* **2019,** *6* (7), 182158.

(24) Parise, J. B.; Cox, D. E., Structural changes occurring upon dehydration of zeolite Rho. A study using neutron powder diffraction and distance-least-squares structural modeling. *J. Phys. Chem.* **1984,** *88* (8), 1635-1640.

(25) Lee, Y.; Reisner, B. A.; Hanson, J. C.; Jones, G. A.; Parise, J. B.; Corbin, D. R.; Toby, B. H.; Freitag, A.; Larese, J. Z., New insight into cation relocations within the pores of zeolite rho: In situ synchrotron X-ray and neutron powder diffraction studies of Pb-and Cd-exchanged rho. *J. Phys. Chem. B* **2001,** *105* (30), 7188-7199.

(26) Reisner, B. A.; Lee, Y.; Hanson, J. C.; Jones, G. A.; Parise, J. B.; Corbin, D. R.; Toby, B. H.; Freitag, A.; Larese, J. Z.; Kahlenberg, V., Understanding negative thermal expansion and 'trap door' cation relocations in zeolite rho. *Chem. Commun.* **2000,** (22), 2221-2222.

(27) Palomino, M.; Corma, A.; Jordá, J. L.; Rey, F.; Valencia, S., Zeolite Rho: a highly selective adsorbent for CO_2/CH_4 separation induced by a structural phase modification. *Chem. Commun.* **2012,** *48* (2), 215-217.

(28) Pera-Titus, M.; Palomino, M.; Valencia, S.; Rey, F., Thermodynamic analysis of framework deformation in Na, Cs-RHO zeolite upon CO_2 adsorption. *PCCP* **2014,** *16* (44), 24391-24400.

(29) Xu, L.; Okrut, A.; Tate, G. L.; Ohnishi, R.; Wu, K.-L.; Xie, D.; Kulkarni, A.; Takewaki, T.; Monnier, J. R.; Katz, A., Cs-RHO Goes from Worst to Best as Water Enhances Equilibrium CO_2 Adsorption via Phase Change. *Langmuir* **2021,** *37* (47), 13903-13908.

(30) Guo, X.; Corbin, D. R.; Navrotsky, A., Thermodynamics of H_2O and CO_2 Absorption and Guest-Induced Phase Transitions in Zeolite RHO. *J. Phys. Chem. C* **2018,** *122* (35), 20366-20376.

(31) Liu, S.; Zhang, P.; Meng, X.; Liang, D.; Xiao, N.; Xiao, F.-S., Cesium-free synthesis of aluminosilicate RHO zeolite in the presence of cationic polymer. *Microporous Mesoporous Mater.* **2010,** *132* (3), 352-356.

(32) Parise, J. B.; Prince, E., The structure of cesium-exchanged zeolite-RhO at 293K and 493K determined from high resolution neutron powder data. *Mater. Res. Bull.* **1983,** *18* (7), 841-852.

(33) Fischer, R. X.; Baur, W.; Shannon, R.; Parise, J.; Faber, J.; Prince, E., New different forms of ammonium loaded and partly deammoniated zeolite rho studied by neutron powder diffraction. *Acta Crystallogr. Sect. C: Cryst. Struct. Commun.* **1989,** *45* (7), 983-989.

(34) Gier, T. E.; Shannon, R. D.; Sonnichsen, G. C.; Corbin, D. R.; Keane Jr, M. Zeolite Rho as catalyst for conversion of methanol and ammonia to dimethylamine. US4806689A, 1985.

(35) Shannon, R.; Keane Jr, M.; Abrams, L.; Staley, R.; Gier, T.; Corbin, D.; Sonnichsen, G., Selective synthesis of dimethylamine over small-pore zeolites. *J. Catal.* **1988,** *113* (2), 367-382.

(36) Ji, Y.; Deimund, M. A.; Bhawe, Y.; Davis, M. E. Organic-Free Synthesis of Small Pore Zeolite Catalysts. U.S. Patent 10173211B2, 2016.

(37) Lozinska, M. M.; Mangano, E.; Mowat, J. P.; Shepherd, A. M.; Howe, R. F.; Thompson, S. P.; Parker, J. E.; Brandani, S.; Wright, P. A., Understanding carbon dioxide adsorption on univalent cation forms of the flexible zeolite Rho at conditions relevant to carbon capture from flue gases. *J. Am. Chem. Soc.* **2012,** *134* (42), 17628-17642.

(38) Balestra, S.; Gutiérrez-Sevillano, J.; Merkling, P.; Dubbeldam, D.; Calero, S., Simulation study of structural changes in zeolite RHO. *J. Phys. Chem. C* **2013,** *117* (22), 11592-11599.

(39) Lozinska, M. M.; Mowat, J. P.; Wright, P. A.; Thompson, S. P.; Jorda, J. L.; Palomino, M.; Valencia, S.; Rey, F., Cation gating and relocation during the highly selective "trapdoor" adsorption of CO_2 on univalent cation forms of zeolite rho. *Chem. Mater.* **2014,** *26* (6), 2052-2061.

(40) Balestra, S. R.; Hamad, S.; Ruiz-Salvador, A. R.; Domínguez–García, V.; Merkling, P. J.; Dubbeldam, D.; Calero, S., Understanding nanopore window distortions in the reversible molecular valve zeolite RHO. *Chem. Mater.* **2015,** *27* (16), 5657-5667.

(41) Lozinska, M. M.; Mangano, E.; Greenaway, A. G.; Fletcher, R.; Thompson, S. P.; Murray, C. A.; Brandani, S.; Wright, P. A., Cation control of molecular sieving by flexible Li-containing zeolite Rho. *J. Phys. Chem. C* **2016,** *120* (35), 19652-19662.

(42) Liang, D.; Hu, Y.; Bao, Q.; Zhang, J.; Feng, J.; Sun, P.; Ma, Y.; Zhang, H., A suitable zeolite Rho for separating CO_2/CH_4 in pressure swing adsorption (PSA) process. *Inorg. Chem. Commun.* **2021,** *127*, 108547.

(43) Lozinska, M. M.; Jamieson, S.; Verbraeken, M. C.; Miller, D. N.; Bode, B.; Murray, C.; Brandani, S.; Wright, P. A., Cation ordering and exsolution in copper-containing forms of the flexible zeolite Rho (Cu,M-Rho; M=H, Na) and their consequences for CO_2 adsorption. *Chem. Eur. J.* **2021,** *27* (51), 13029-13039.

(44) Neilsen, G.; Dickson, M. S.; Rosen, P. F.; Guo, X.; Navrotsky, A.; Woodfield, B. F., Heat capacity and thermodynamic functions of partially dehydrated cation-exchanged (Na^+, Cs^+, Cd^{2+}, Li^+, and NH^{4+}) RHO zeolites. *J. Chem. Thermodyn.* **2021**, 106620.

(45) Petříček, V.; Dušek, M.; Palatinus, L., Crystallographic computing system JANA2006: general features. *Z. Kristallogr. - Cryst. Mater.* **2014,** *229* (5), 345-352.

(46) Ghojavand, S.; Clatworthy, E. B.; Vicente, A.; Dib, E.; Ruaux, V.; Debost, M.; El Fallah, J.; Mintova, S., The role of mixed alkali metal cations on the formation of nanosized CHA zeolite from colloidal precursor suspension. *J. Colloid Interface Sci.* **2021,** *604*, 350-357.

(47) Nearchou, A.; Sartbaeva, A., Influence of alkali metal cations on the formation of zeolites under hydrothermal conditions with no organic structure directing agents. *CrystEngComm* **2015,** *17* (12), 2496-2503.

(48) Robson, H. E. ZEOLITE RHO. US3904738A, 1973.

(49) Chatelain, T.; Patarin, J.; Fousson, E.; Soulard, M.; Guth, J.; Schulz, P., Synthesis and characterization of high-silica zeolite RHO prepared in the presence of 18-crown-6 ether as organic template. *Microporous Mater.* **1995,** *4* (2-3), 231-238.

(50) Shang, J.; Li, G.; Singh, R.; Gu, Q.; Nairn, K. M.; Bastow, T. J.; Medhekar, N.; Doherty, C. M.; Hill, A. J.; Liu, J. Z.; Webley, P. A., Discriminative separation of gases by a "molecular trapdoor" mechanism in chabazite zeolites. *J. Am. Chem. Soc.* **2012,** *134* (46), 19246-19253.

(51) Shang, J.; Li, G.; Singh, R.; Xiao, P.; Liu, J. Z.; Webley, P. A., Determination of composition range for "molecular trapdoor" effect in chabazite zeolite. *J. Phys. Chem. C* **2013,** *117* (24), 12841-12847.

(52) Li, G. K.; Shang, J.; Gu, Q.; Awati, R. V.; Jensen, N.; Grant, A.; Zhang, X.; Sholl, D. S.; Liu, J. Z.; Webley, P. A., Temperature-regulated guest admission and release in microporous materials. *Nat. Commun.* **2017,** *8* (1), 1-9.

(53) Coudert, F.-X.; Kohen, D., Molecular insight into CO_2 "trapdoor" adsorption in zeolite Na-RHO. *Chem. Mater.* **2017,** *29* (7), 2724-2730.

(54) Zhao, J.; Mousavi, S. H.; Xiao, G.; Mokarizadeh, A. H.; Moore, T.; Chen, K.; Gu, Q.; Singh, R.; Zavabeti, A.; Liu, J. Z.; Webley, P. A.; Li, G. K., Nitrogen Rejection from Methane via a "Trapdoor" K-ZSM-25 Zeolite. *J. Am. Chem. Soc.* **2021,** *143* (37), 15195–15204.

(55) McCusker, L. B.; Baerlocher, C. In *The effect of dehydration upon the crystal structure of zeolite Rho*, Proceedings of the Sixth International Zeolite Conference, Reno, United States of America, Olson, D.; Attilio, B., Eds. Butterworths: Reno, United States of America, 1983; pp 812-822.

(56) Lapshin, A.; Golubeva, O. Y., Distribution of extra-framework cations and water molecules in synthetic high-silica (Na, Cs)-rho-zeolite. *Glass Phys. Chem* **2013,** *39* (4), 420-424.

(57) Baur, W. H.; Bieniok, A.; Shannon, R. D.; Prince, E., Neutron powder diffraction study of a Na, Cs-Rho zeolite. *Z. Kristallogr. - Cryst. Mater.* **1989,** *187* (1-4), 253-266.

(58) Guo, X.; Wu, L.; Corbin, D. R.; Navrotsky, A., Thermochemistry of formation of ion exchanged zeolite RHO. *Microporous Mesoporous Mater.* **2019,** *274*, 373-378.

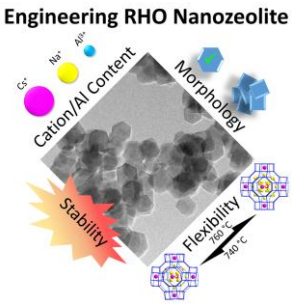
Engineering RHO Nanozeolite
Cs+
Na+
Al3+
Cation/Al Content
Morphology
Stability
Flexibility
360 °C
40 °C